EFFECT OF CALCIUM CARBONATE ON THE MECHANICAL PROPERTIES OF POLYAMIDE 6/ACRYLONITRILE BUTADIENE STYRENE COMPOUNDS WITH STYRENE-ETHYLENE/BUTYLENE-STYRENE

Le Duong (1)

(1) Institute of Engineering and Technology, Thu Dau Mot University
Corresponding author's email: duongl@tdmu.edu.vn

DOI: 10.37550/tdmu.EJS/2026.01.707

Article Info

Volume: 8
Issue: 1
March: 2026
Received: Sep. 25th, 2025
Accepted: Mar. 5th, 2026
Page No: 184-197

Abstract

This study evaluates the effect of Calcium carbonate ($CaCO_3$) on the mechanical properties and structure of SEBS-compatible PA6/ABS composites. Composites consisting of 50/50 PA6/ABS, 5% SEBS, and 0–20% by weight $CaCO_3$ were fabricated by injection molding. Tensile and flexural strengths were determined according to ISO 527-2:2012 and ISO 178:2019, respectively. The tensile strength increased with filler content, peaking at 15 wt% $CaCO_3$ (24.72 MPa), while flexural strength reached a maximum at 10 wt% (32.51 N/mm2). FESEM revealed a uniform dispersion of $CaCO_3$ particles and strong interfacial adhesion at optimal filler contents, whereas agglomeration and microvoids occurred at higher loadings. The results demonstrate that moderate $CaCO_3$ addition enhances stiffness and strength through effective stress transfer, while excessive loading induces brittleness due to poor interfacial bonding. This study contributes to the optimization of hybrid polymer composites for structural, automotive and precision engineering.

Keywords: calcium carbonate; flexural strength; PA6/ABS compound; styrene-ethylene/butylene-styrene (SEBS); tensile strength.

1. Introduction

In recent years, the demand for light yet high-strength materials has increased significantly in many industrial sectors, particularly aerospace and construction. Traditional polymer materials often fail to meet the stringent mechanical requirements of these applications. Therefore, many advanced material solutions have been researched and developed to improve material performance, with composites emerging as an effective approach. Thanks to the combination of different material phases, composites demonstrate superior advantages in strength, stiffness, and deformation resistance, contributing to a wider range of applications compared to traditional materials (Essabir et al., 2018; Qaiss et al., 2015).

Polyamide 6 (PA6) is a high-tensile-strength plastic widely used across various industries due to its semi-crystalline structure, good resistance to plastic deformation, thermal stability, and effective chemical resistance (Karsli et al., 2013). However, PA6 also has some drawbacks, such as high hygroscopicity and the potential for brittleness and crumbling at low temperatures. Therefore, it needs to be combined with other thermoplastic polymers to overcome these disadvantages (Karsli et al., 2013). Meanwhile, acrylonitrile-butadiene-styrene (ABS) is a material with good dimensional stability, but this stability decreases significantly at high temperatures, and ABS also exhibits limited mechanical properties, especially low tensile and flexural strengths (Li et al., 2009; Mohammadian-Gezaz et al., 2009). Therefore, combining PA6 with ABS is considered a potential approach to creating a new material system with a better balance of mechanical properties and thermal performance, as has been mentioned and demonstrated in several previous studies (Liu et al., 2013; Arsad et al., 2011).

However, some studies indicate that during blending of PA6 with ABS, relatively large butadiene-rich domains can form significantly reducing the impact strength of the material system (Sharma et al., 2020). To overcome this phenomenon and reduce the incompatibility between the two polymers, a standard solution is to improve interaction and adhesion at the phase boundary by adding a third component as an adjuvant, thereby reducing the surface tension between the phases (Shen et al., 2013). Among the compatibilizers studied, SEBS (styrene-ethylene/butylene-styrene) is noted for its ability to more effectively control phase size and significantly improve impact strength, thus enhancing the compatibility of PA6/ABS (Essabir et al., 2020).

Recent research highlights the crucial role of elastomer-grafted compatibilizers in enhancing multiphase polymer blends by reducing interfacial tension and promoting fine morphology development, which leads to significant improvements in both strength and toughness. For example, elastomer-grafted SEBS and POE compatibilizers with reactive functional groups (such as maleic anhydride and glycidyl methacrylate) have been shown to dramatically enhance interfacial adhesion in complex blend systems, leading to ultrafine microstructures and unexpected simultaneous growth in tensile strength and impact toughness due to hierarchical interfacial interactions and energy dissipation mechanisms at interfaces (Yan et al., 2024). Similarly, recent reviews on thermoplastic elastomers grafted compatibilizers demonstrate that incorporating reactive compatibilizers such as SEBS-g-MAH into immiscible blends enhances compatibility and stress transfer, broadening the design space for high-performance engineering composites (Xu et al., 2025). These advances illustrate that compatibilizer chemistry and architecture, especially in multi-phase systems with SEBS and reactive groups, play a determining role in governing morphology-property relationships, beyond simple filler content effects.

Besides using compatibilizers, the mechanical properties of polymers can be effectively improved by selecting suitable fillers, among which glass fibre (GF), clay, Calcium carbonate ($CaCO_3$), and silica have been extensively studied. GF and $CaCO_3$ are often preferred in blended polymer systems due to their ability to reduce costs, increase stiffness and mechanical strength, while still ensuring the recyclability of the material. Nano-sized $CaCO_3$ (44 nm) has been applied in PVC nanocomposite systems at concentrations of 2.5–7.5% by weight, showing that the uniform dispersion of filler particles helps form effective bonds with the polymer matrix, thereby simultaneously improving the toughness and stiffness of the material (Xie et al., 2004). For the

PA6/ABS/$CaCO_3$ system, tensile strength is significantly improved with the addition of micrometer-sized $CaCO_3$, with the optimal value achieved at a $CaCO_3$ content of 5%, representing an increase of approximately 75% compared to the unfilled PA6/ABS system (Karsli et al., 2013). Recent work on similar immiscible polymer composites shows that compatibilization and filler dispersion are intimately linked; effective compatibilizers can dramatically reduce dispersed phase size and stabilize filler distribution, resulting in significant mechanical improvements compared to uncompatibilized materials, even at low compatibilizer concentrations (Du et al., 2025). Furthermore, carbon fiber and glass fiber-reinforced PA6-based composites, fabricated using the TRTM method with caprolactam, also show significant reinforcement efficiency, with efficiencies of 44% for carbon fiber and 26% for glass fiber, respectively (Zaldua et al., 2019). Compared with other polymers, ABS is a low-cost polymer, and when blended with PA6, it contributes to improved mechanical strength and dimensional stability of the composite, thereby expanding the practical application potential of this material system (Majumdar et al., 1994).

A review of previous studies indicates that improving the mechanical strength of materials is a key factor. Based on this, this study focuses on investigating the PA6/ABS system supplemented with $CaCO_3$ at different concentrations, while optimizing the fabrication and processing conditions to clarify the influence of $CaCO_3$ on tensile strength, flexural strength, and microstructural characteristics of the material.

2. Materials and methods

In this study, a PA6/ABS material system with a 50/50 mixing ratio was used, modified with SEBS at a fixed 5% by weight. $CaCO_3$ filler was added at varying levels, ranging from 0 to 20% by weight, according to the formulations presented in Table 1. The starting materials, including PA6, ABS, and SEBS, were all supplied by Kim Hoang Long Co., Ltd. (Vietnam).

Table 1. Content of the samples (wt. %)

No.	Ingredient (wt. %)			
	PA6	**ABS**	**$CaCO_3$**	**SEBS**
1	47.5	47.5	0	5
2	42.5	42.5	5	5
3	40.0	40.0	10	5
4	37.5	37.5	15	5
5	35.0	35.0	20	5

(Source: Author, 2025)

All materials (PA6, ABS, and $CaCO_3$) were dried at 80°C for one hour prior to processing to remove residual moisture. The dried mixtures were then processed using a SHINE W120B injection molding machine (Figure 1).

Figure 1. Injection molding machine SW-120B

Source: Laboratory Work, 2025

The specimens used for tensile testing were fabricated according to ISO 527-2:2012, with specimens measuring 168 mm × 20 mm × 4 mm, as illustrated in Figure 2. To analyze the effect of $CaCO_3$ content, each material formulation was tested on five independent specimens. Before experimenting, all specimens were conditioned under standard conditions at 23 ± 2 °C and 50 ± 5% relative humidity and then installed in the tensile testing system as shown in Figure 3. The experiments were conducted at room temperature, with the tensile speed kept constant at 50 mm/min, using a non-contact strain gauge (without a camera) with a resolution of 1.8 µm, integrated into a Shimadzu AG-X Plus 20 kN tensile testing machine (Japan). The test system is built based on the following technical specifications: a maximum test force of 20 kN, a speed range of 0.001 to 1600 mm/min, a speed accuracy of ± 0.1%, an operating temperature range of 5 to 50°C, and a data acquisition frequency of 1000 Hz.

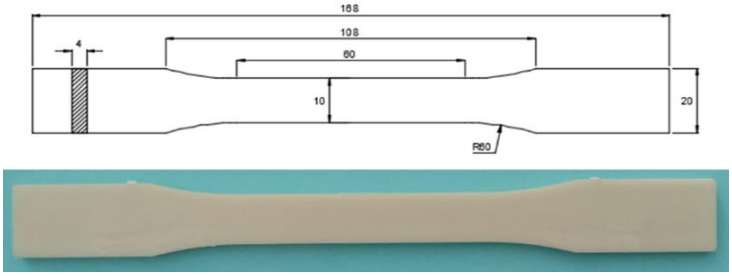

Figure 2. Tensile strength test sample

Source: Author, 2025

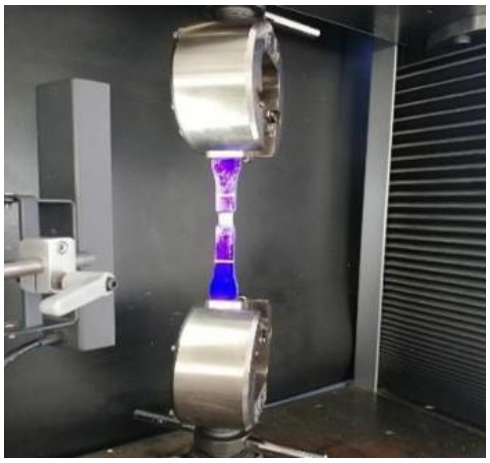

Figure 3. Shimadzu AG-X Plus machine

Source: Laboratory Work, 2025

The bending test was conducted according to ISO 178:2019, with specimens measuring 129 mm × 12 mm × 3.2 mm, as illustrated in Figure 4. For each formulation, five test specimens were used to evaluate the effect of $CaCO_3$ content. Before testing, the samples were stabilized at a temperature of 23 ± 2°C and a relative humidity of 50 ± 5%. Tests were conducted at room temperature with a constant test velocity of 1,408 mm/min using a Shimadzu AG-X Plus 20 kN machine (Japan) where the equipment specifications and measurement conditions were equivalent to those of the tensile test.

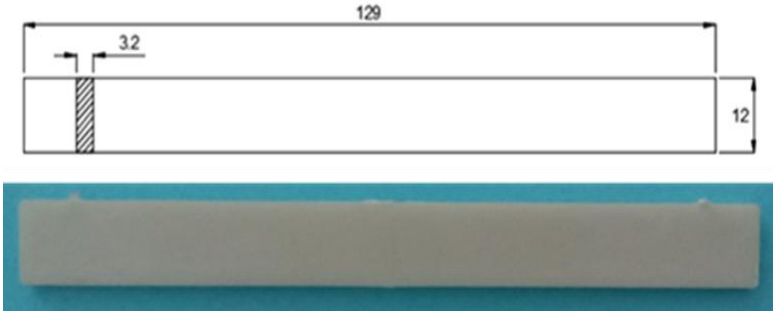

Figure 4. Flexural strength test sample

Source: Author, 2025

After completing the tensile and bending processes, the specimens were examined for surface cracks using an electron microscope, which scanned the field emission with an acceleration voltage of 10 kV, as shown in Figure 5. This method allows for detailed observation of the microstructure of the fracture zone, while also evaluating the dispersion and interaction of the filler in the polymer matrix. To ensure image quality and avoid interference due to charge accumulation, the sample surface was coated with a thin layer of platinum, approximately 3–5 nm thick, before observation.

Figure 5. Electron microscope (FESEM) Hitachi S-4800 (Japan)

Source: Laboratory Work, 2025

3. Results and Discussion

3.1. Tensile strength of PA6/ABS compound in each CaCO3 filler

Table 2 summarizes the tensile strength values of PA6/ABS/SEBS composites containing various $CaCO_3$ loadings, and the corresponding trend is illustrated in Figure 6.

At 0 wt% $CaCO_3$, corresponding to the unfilled PA6/ABS/SEBS blend, the average tensile strength is 22.35 MPa. A marginal increase to 22.83 MPa is observed at 5 wt% $CaCO_3$, which remains within one standard deviation and therefore indicates only a limited reinforcing effect at low filler loading. When the $CaCO_3$ content is increased to 10 wt%, the tensile strength increases markedly to 24.56 MPa, followed by a further increase to a maximum value of 24.72 MPa at 15 wt% $CaCO_3$. In contrast, a pronounced decrease in tensile strength is recorded at 20 wt% $CaCO_3$, where the average value drops to 19.17 MPa, accompanied by a large standard deviation (3.86 MPa), suggesting increased structural heterogeneity.

These results demonstrate that $CaCO_3$ content has a significant influence on the tensile performance of the PA6/ABS/SEBS system, with an optimal filler range between 10 and 15 wt%. A similar non-monotonic trend has been widely reported for PA6- and ABS-based composites reinforced with mineral fillers, where moderate filler loadings improve tensile strength, while excessive contents lead to deterioration due to dispersion-related issues. For example, Karsli et al. (2013) reported that micrometer-sized $CaCO_3$ improved the tensile strength of ABS/PA6 composites up to an optimal loading, beyond which tensile performance declined due to particle agglomeration and weakened matrix continuity. Likewise, Xie et al. (2004) observed that $CaCO_3$-filled polymer systems exhibit enhanced tensile properties only within a limited filler range, as excessive filler loading introduces stress concentration sites.

Compared with uncompatibilized PA6/ABS systems reported in the literature, where tensile strength often decreases rapidly at higher filler contents due to poor interfacial adhesion (Mohammadian-Gezaz et al., 2009; Majumdar et al., 1994), the present PA6/ABS/SEBS system maintains relatively high tensile strength up to 15 wt% $CaCO_3$. This observation suggests that the presence of SEBS at a fixed content of 5 wt% contributes to mitigating the negative effects typically associated with filler addition, although direct interfacial measurements were not performed in this study.

From a mechanistic standpoint, the tensile behavior can be interpreted in terms of filler reinforcement efficiency and matrix continuity. At $CaCO_3$ contents up to 15 wt%, rigid filler particles contribute to load sharing under tensile deformation, resulting in an increase in average tensile strength. This reinforcing effect is consistent with observations reported by Essabir et al. (2018), who showed that improved stress distribution in compatibilized PA6/ABS systems leads to enhanced tensile performance. However, the magnitude of improvement remains moderate (approximately 10.6% increase from 0 to 15 wt% $CaCO_3$), indicating that reinforcement is limited by the intrinsic stiffness contrast between $CaCO_3$ and the polymer matrix.

When the $CaCO_3$ content reaches 20 wt%, the sharp reduction in tensile strength, together with the increased scatter in measured values, indicates a loss of structural homogeneity. Similar behavior has been reported by Karsli et al. (2013) and Altan (2010), who attributed tensile degradation at high filler contents to particle agglomeration and insufficient wetting by the polymer matrix, leading to premature failure under tensile loading. In the present system, the data suggest a transition from a reinforcement-dominated regime ($\leq$15 wt% $CaCO_3$) to a defect-dominated regime at higher filler loadings.

Overall, the tensile results confirm that $CaCO_3$ can enhance the tensile strength of PA6/ABS/SEBS composites within a limited concentration window. While the improved

tensile performance at 10-15 wt% $CaCO_3$ is consistent with trends reported in previous studies, the present results demonstrate that this optimal range is preserved in a SEBS-compatibilized PA6/ABS matrix under the selected processing conditions. Further quantitative interfacial or morphological analysis would be required to establish a direct correlation between tensile strength and interfacial adhesion strength.

Table 2. Tensile strength measurement results

No.	Tensile strength (MPa)				
	1	2	3	4	5
1	22.15	22.39	24.11	23.27	21.00
2	23.08	23.02	23.32	28.20	13.04
3	22.40	22.67	25.16	23.20	17.77
4	22.05	23.16	25.37	25.62	21.53
5	22.07	22.91	24.85	23.30	22.51
Average	22.35	22.83	24.56	24.72	19.17
Standard deviation	0.43	0.30	0.84	2.20	3.86

Source: Author, 2025

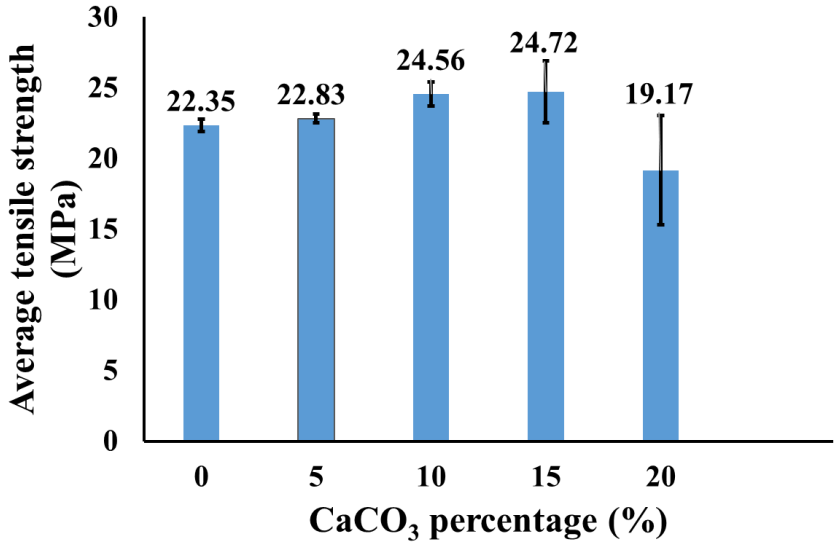

Figure 6. Tensile strength of the PA6/ABS compound at each $CaCO_3$ content

Source: Author, 2025

Table 3 presents the one-way ANOVA results for tensile strength. Statistical analysis confirms a significant effect of $CaCO_3$ content on tensile strength ($p = 0.002$). Approximately 54.84% of the total variation in tensile strength is explained by changes in filler concentration. Tukey's post-hoc test indicates that composites containing 10 - 15 wt% $CaCO_3$ exhibit significantly higher tensile strength than both the unfilled and 20 wt% $CaCO_3$ samples ($p < 0.05$), supporting the existence of an optimal filler range. These findings are consistent with previous studies reporting enhanced tensile performance at moderate mineral filler loadings and degradation at excessive contents due to poor dispersion and matrix discontinuity (Zhao et al., 2022; Altan, 2010).

Table 3. ANOVA analysis results of the ABS/PA6/ $CaCO_3$ samples

Source	DF	SS	MS	F	P
Sample	4	100.68	25.17	6.07	0.002
Error	20	82.92	4.15		
Total	24	183.60			
S = 2.036		R – Sq = 54.84%		R – Sq (adj) = 45.81%	

Source: Author, 2025

3.2. Flexural strength of PA6/ABS compound in each CaCO3 fille

The flexural strength results are summarized in Table 4 and illustrated in Figure 7. The unfilled PA6/ABS/SEBS composite exhibits an average flexural strength of 30.48 MPa. The addition of 5 wt% $CaCO_3$ results in a moderate increase to 31.25 MPa, while the highest flexural strength of 32.51 MPa is achieved at 10 wt% $CaCO_3$. Further increasing the $CaCO_3$ content to 15 wt% causes a reduction in flexural strength to 29.53 MPa, followed by a more pronounced decrease to 25.57 MPa at 20 wt%.

A similar non-linear dependence of flexural strength on $CaCO_3$ content has been reported in previous studies on PA6- and ABS-based composites. Karsli et al. (2013) observed that micrometer-sized $CaCO_3$ enhances flexural strength at moderate loadings due to improved stiffness, whereas excessive filler addition leads to particle agglomeration and reduced bending resistance. Likewise, Ramesh and Panneerselvam (2021) reported that flexural properties of injection-molded polymer composites exhibit an optimal filler window, beyond which flexural strength deteriorates due to stress concentration and microvoid formation.

Compared with tensile behavior, the flexural response exhibits a narrower optimal filler window and a more pronounced sensitivity to excessive $CaCO_3$ loading. While tensile strength reaches its maximum at 15 wt% $CaCO_3$, flexural strength peaks at a lower filler content (10 wt%), indicating that bending performance is more sensitive to microstructural discontinuities.

Under flexural loading, the composite experiences simultaneous tensile and compressive stresses, making interfacial stability and crack resistance particularly critical. The enhanced flexural strength observed at 10 wt% $CaCO_3$ suggests that this filler concentration provides sufficient stiffness enhancement without compromising matrix continuity. In this regime, $CaCO_3$ particles effectively constrain deformation, while the elastomeric SEBS phase dissipates strain energy through localized plastic deformation, suppressing microcrack initiation at the filler–matrix interface.

This behavior is consistent with the findings of Essabir et al. (2020), who demonstrated that SEBS-compatibilized PA6/ABS blends exhibit improved resistance to bending-induced damage due to enhanced interfacial stability and energy dissipation capability. In addition, Majumdar et al. (1994) reported that elastomer-modified PA6/ABS systems show superior flexural performance at moderate filler contents, where the balance between stiffness and toughness is optimized.

At higher $CaCO_3$ contents (≥15 wt%), agglomerated particles act as rigid inclusions that intensify stress gradients under bending, accelerating interfacial debonding and crack

growth. Although SEBS contributes to stress relaxation, its toughening efficiency diminishes when the filler content exceeds the percolation limit of the polymer matrix. As a result, flexural strength declines more sharply than tensile strength at excessive $CaCO_3$ loading, highlighting the higher sensitivity of bending performance to microstructural heterogeneity.

Similar flexural strength degradation at high mineral filler loadings has been reported by Zhao et al. (2022), who attributed the reduction in bending performance to heterogeneous filler dispersion and the formation of stress concentration zones during injection molding. These observations further support the interpretation that flexural properties are particularly sensitive to filler agglomeration and matrix continuity in multiphase polymer systems.

Table 4. Flexural strength measurement results

No.	Tensile strength (MPa)				
	1	2	3	4	5
1	32.87	36.49	35.58	27.19	24.16
2	29.16	28.01	30.11	26.67	29.91
3	31.81	33.4	34.63	29.85	22.06
4	28.42	34.12	32.08	31.19	24.18
5	30.15	24.23	30.15	32.76	27.54
Average	30.48	31.25	32.51	29.53	25.57
Standard deviation	1.84	5.0	2.52	2.6	3.12

Source: Author, 2025

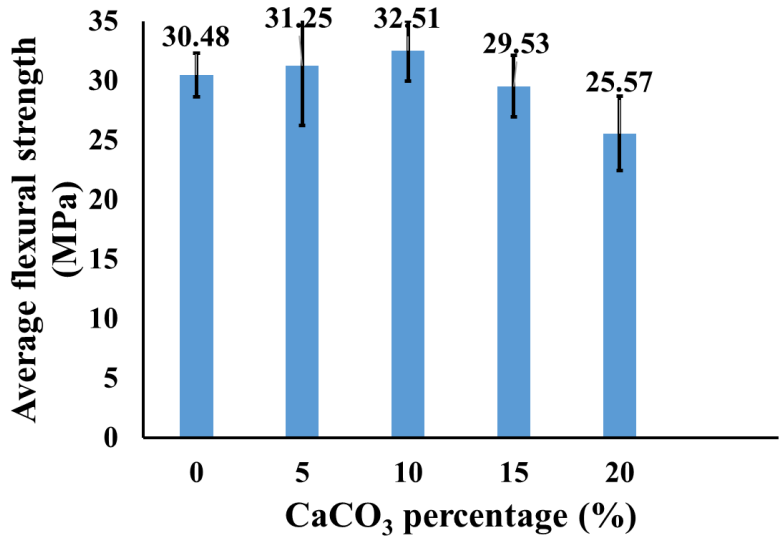

Figure 7. Flexural strength of the PA6/ABS compound at each CaCO3 content.

Source: Author, 2025

ANOVA results for flexural strength (Table 5) confirm a statistically significant influence of $CaCO_3$ content ($p = 0.028$), with 40.45% of the total variation explained by filler concentration. Tukey's test indicates that the 10 wt% $CaCO_3$ composite exhibits significantly higher flexural strength than the 0 wt% and 20 wt% samples ($p < 0.05$). These results are consistent with previous studies reporting improved bending strength at moderate $CaCO_3$ loadings and deterioration at higher contents due to stress concentration and microvoid formation (Zhao et al., 2022; Ramesh & Panneerselvam, 2021).

Table 5. ANOVA analysis results of the ABS/PA6/ $CaCO_3$ samples.

Source	DF	SS	MS	F	P
Sample	4	139.3	34.8	3.40	0.028
Error	20	205.0	10.3		
Total	24	344.3			
S = 3.202		R – Sq = 40.45%		R – Sq (adj) = 28.54%	

Source: Author, 2025

3.3. Microstructure

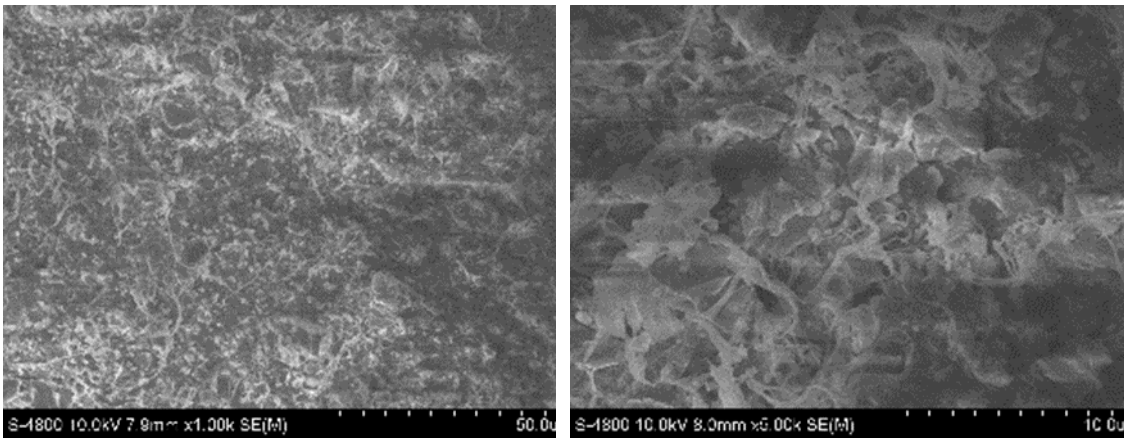

Figure 8. The sample has maximum tensile strength

Source: Author, 2025

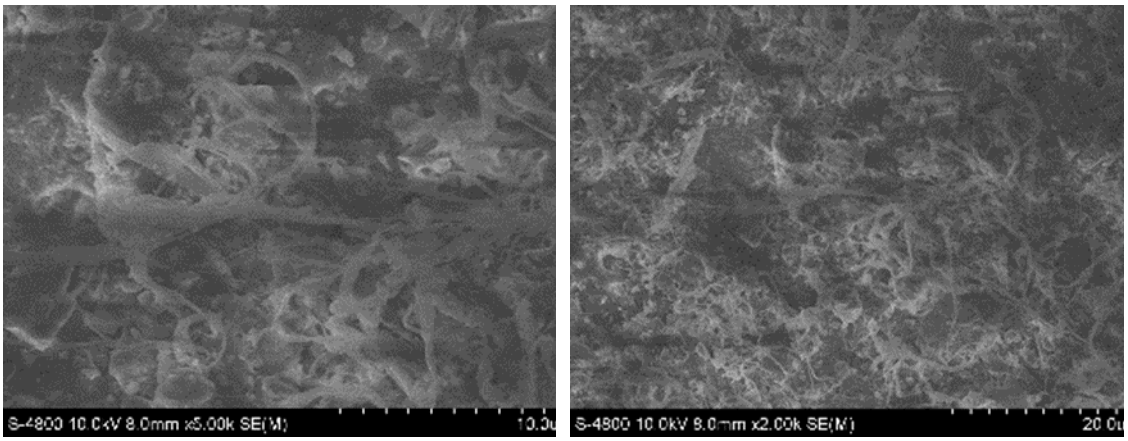

Figure 9. The sample has maximum flexural strength

Source: Author, 2025

Figures 8 and 9 present FESEM images of the PA6/ABS/SEBS composites corresponding to the maximum tensile and flexural strengths, respectively. At $CaCO_3$ contents of 10 - 15 wt%, the filler particles are finely and uniformly dispersed within the polymer matrix, accompanied by strong interfacial adhesion and limited void formation. These uniformly distributed particles act as effective stress-transfer sites between PA6 and ABS domains. The presence of SEBS further enhances interfacial bonding by reducing surface tension between the polar PA6 and non-polar ABS phases, thereby improving filler wetting and interphase continuity. Similar morphological features have been reported in compatibilized polymer blends exhibiting improved mechanical performance (Huang et al., 2023; Donato et al., 2022).

When the $CaCO_3$ content exceeds 15 wt%, pronounced particle agglomeration and micropore formation are observed. These defects act as stress concentrators and preferential crack initiation sites under mechanical loading, leading to premature failure. This behavior is consistent with previous findings demonstrating that excessive mineral filler content results in poor dispersion and brittle fracture due to particle clustering (Zhao et al., 2022; Tanaka et al., 2023).

Notably, the SEM observations provide direct microstructural evidence for the synergistic reinforcement mechanism in the PA6/ABS/SEBS/$CaCO_3$ system. At optimal filler contents (10 - 15 wt%), SEBS promotes the formation of a more continuous and compliant interphase among PA6, ABS, and $CaCO_3$ particles, reducing interfacial debonding and suppressing crack initiation. In contrast, at high filler loadings, this interphase-mediated stress redistribution becomes less effective, and filler particles increasingly behave as defect sites rather than reinforcements. Consequently, the superior mechanical performance observed in this study arises from the combined effects of controlled $CaCO_3$ dispersion and SEBS-induced interfacial stabilization, rather than filler addition alone.

Although the FESEM analysis in this work is primarily qualitative, the strong consistency between mechanical trends and observed microstructural features supports the proposed structure–property relationships. Quantitative image analysis (e.g., particle size distribution or void fraction) was not conducted and is recognized as a limitation of the present study. Future work will focus on integrating quantitative SEM analysis with complementary techniques such as differential scanning calorimetry (DSC) to evaluate crystallinity changes and dynamic mechanical analysis (DMA) to elucidate viscoelastic behavior and interphase damping mechanisms, thereby providing a more comprehensive understanding of the reinforcement mechanisms in PA6/ABS/SEBS/$CaCO_3$ composites.

4. Conclusions

This study systematically investigated the influence of $CaCO_3$ content on the mechanical performance and microstructural characteristics of PA6/ABS blends compatibilized with SEBS. The experimental results clearly demonstrate that $CaCO_3$ acts as an effective reinforcing filler within a specific concentration window. The tensile strength of the composites increased from 22.35 MPa for the unfilled system to a maximum value of 24.72 MPa at 15 wt% $CaCO_3$, while the flexural strength reached its highest value of 32.51 MPa at 10 wt% $CaCO_3$. These distinct optimal contents for tensile and flexural loading highlight the sensitivity of different deformation modes to filler dispersion and interfacial stability.

FESEM observations revealed that the enhancement in mechanical properties at moderate $CaCO_3$ contents (10 - 15 wt%) is associated with the uniform dispersion of filler particles and strong interfacial adhesion between $CaCO_3$ and the PA6/ABS matrix. In contrast, excessive $CaCO_3$ loading (>15 wt%) resulted in particle agglomeration and microvoid formation, which acted as stress concentrators and led to premature failure, thereby reducing both strength and ductility.

Beyond confirming general filler–property trends reported in polymer composites, this work provides specific insight into the synergistic role of SEBS compatibilization in the PA6/ABS/$CaCO_3$ system. The presence of SEBS at a fixed content of 5 wt% promotes interfacial stabilization between the polar PA6 phase, the non-polar ABS phase, and the inorganic $CaCO_3$ filler, enabling efficient stress transfer and delaying filler-induced embrittlement. As a result, the composite can tolerate relatively high $CaCO_3$ loadings (up to 15 wt%) while maintaining improved mechanical performance. This finding underscores the importance of compatibilizer-assisted morphology control in multiphase polymer systems.

From an application perspective, the optimized PA6/ABS/SEBS/$CaCO_3$ formulation represents a cost-effective and lightweight alternative to fiber-reinforced composites for semi-structural components, where moderate stiffness enhancement, dimensional stability, and good processability via injection molding are required. Potential application fields include automotive interior parts, electrical housing, and general engineering components.

Although the present study establishes clear structure–property relationships based on mechanical testing and qualitative microstructural analysis, further investigations are required to deepen the mechanistic understanding. Future work should focus on incorporating surface-treated or nano-sized $CaCO_3$ fillers, as well as complementary characterization techniques such as rheological analysis, differential scanning calorimetry (DSC), and dynamic mechanical analysis (DMA). In addition, systematic variation of compatibilizer type and content, along with long-term durability and thermal aging studies, would further support the development and industrial implementation of advanced PA6/ABS-based composite materials.

References

Essabir, H., Rodrigue, D., Bouhfid, R., & Qaiss, A. E. K. (2018). *Effect of nylon 6 (PA 6) addition on the properties of glass fiber reinforced acrylonitrile-butadiene-styrene*. Polymer Composites, 39(1), 14-21.

Qaiss, A., Bouhfid, R., & Essabir, H. (2015). *Characterization and use of coir, almond, apricot, argan, shells, and wood as reinforcement in the polymeric matrix in order to valorize these products*. Agricultural biomass based potential materials, 305-339.

Karsli, N. G., & Aytac, A. (2013). *Tensile and thermomechanical properties of short carbon fiber reinforced polyamide 6 composites.* Composites Part B: Engineering, 51, 270-275.

Karsli, N. G., Yilmaz, T., Aytac, A., & Ozkoc, G. (2013). *Investigation of erosive wear behavior and physical properties of SGF and/or calcite reinforced ABS/PA6 composites*. Composites Part B: Engineering, 44(1), 385-393.

Li, J., & Zhang, Y. F. (2009). *Tensile strength of ABS/PA6 composites reinforced with HNO 3-treated carbon fibers*. Mechanics of Composite Materials, 45, 537-542.

Mohammadian-Gezaz, S., Ghasemi, I., & Oromiehie, A. (2009). *Study of the properties of compatibilized ABS/PA6 blends using response surface methodology*. Journal of Vinyl and Additive Technology, 15(3), 191-198.

Liu, X. Q., Bao, R. Y., Liu, Z. Y., Yang, W., Xie, B. H., & Yang, M. B. (2013). *Effect of nano-silica on the phase inversion behavior of immiscible PA6/ABS blends*. Polymer testing, 32(1), 141-149.

Arsad, A., Rahmat, A. R., Hassan, A., & Iskandar, S. N. (2011). *Mechanical and rheological characterization of PA6 and ABS blends-with and without short glass fiber*. J Appl Sci, 11(13), 2313-2319.

Sharma, V., Kapoor, S., Goyal, M., & Jindal, P. (2020). *Enhancement of the mechanical properties of graphene-based acrylonitrile butadiene styrene (ABS) nanocomposites*. Materials Today: Proceedings, 28, 1744-1747.

Shen, J., Piunova, V. A., Nutt, S., & Hogen-Esch, T. E. (2013). *Blends of polystyrene and poly (n-butyl methacrylate) mediated by perfluorocarbon end groups*. Polymer, 54(21), 5790-5800.

Essabir, H., El Mechtali, F. Z., Nekhlaoui, S., Raji, M., Bensalah, M. O., Rodrigue, D.,... & Qaiss, A. (2020). *Compatibilization of PA6/ABS blend by SEBS-g-MA: morphological, mechanical, thermal, and rheological properties*. The International Journal of Advanced Manufacturing Technology, 110, 1095-1111.

Yan, J., Wang, C., Zhang, T., Xiao, Z., & Xie, X. (2024). Super Tough PA6/PP/ABS/SEBS Blends Compatibilized by a Combination of Multi-Phase Compatibilizers. Materials, 17(21), 5370.

Xu, Y., Yao, X., Zhang, Z., Zhu, D., Na, H., Jin, Z., & Fang, C. (2025). Recent research progress and applications of thermoplastic elastomers grafted compatibilizers in polymer blends and composites. Materials Today Communications, 111500.

Xie, X. L., Liu, Q. X., Li, R. K. Y., Zhou, X. P., Zhang, Q. X., Yu, Z. Z., & Mai, Y. W. (2004). *Rheological and mechanical properties of PVC/$CaCO_3$ nanocomposites prepared by in situ polymerization*. Polymer, 45(19), 6665-6673.

Du, J. N., Wei, W. K., Lu, S. D., & Wang, D. (2025). Compatibilizer-aided Fabrication of a 'High-entropy Polymer Blend'. Chinese Journal of Polymer Science, 43(9), 1592-1601.

Zaldua, N., Maiz, J., de la Calle, A., García-Arrieta, S., Elizetxea, C., Harismendy, I., ... & Müller, A. J. (2019). *Nucleation and crystallization of PA6 composites prepared by T-RTM: Effects of carbon and glass fiber loading*. Polymers, 11(10), 1680.

Majumdar, B., Keskkula, H., & Paul, D. R. (1994). *Mechanical properties and morphology of nylon-6/acrylonitrile-butadiene-styrene blends compatibilized with imidized acrylic polymers*. Polymer, 35(25), 5453-5467.

Zhao, N. Y., Lian, J. Y., Wang, P. F., & Xu, Z. B. (2022). *Recent progress in minimizing the warpage and shrinkage deformations by the optimization of process parameters in plastic injection molding: A review*. The International Journal of Advanced Manufacturing Technology, 120(1), 85-101.

Altan, M. (2010). *Reducing shrinkage in injection moldings via the Taguchi, ANOVA and neural network methods*. Materials & Design, 31(1), 599-604.

Ramesh, M., & Panneerselvam, K. (2021, September). *Optimization for Injection Moulding process parameters towards Warpage and Shrinkage of HDPE-PBI composites*. In IOP Conference Series: Materials Science and Engineering (Vol. 1183, No. 1, p. 012001). IOP Publishing.

Huang, H., Liu, W., & Liu, Z. (2023). *Additive manufacturing-inspired approach to re-manufacture fiber reinforced plastic with programmable orientation of recycled carbon fiber*. Composites Communications, 38, 101521.

Donato, A., Belluzzi, E., Mattiuzzo, E., Venerando, R., Cadamuro, M., Ruggieri, P., ... & Brun, P. (2022). *Anti-inflammatory and pro-regenerative effects of hyaluronan-chitlac mixture in human dermal fibroblasts: a skin ageing perspective*. Polymers, 14(9), 1817.

Tanaka, R., Ajala, O. A., Nakayama, Y., & Shiono, T. (2023). *Control of coordination polymerization behavior by counter-anionic effects*. Progress in Polymer Science, 142, 101690.